IL NUOVO CIMENTO **44 C** (2021) 14
DOI 10.1393/ncc/i2021-21014-9

COMMUNICATIONS: SIF Congress 2020

Modelling surface displacement in restless hydrothermal regions: The case of a thermo-poro-elastic inclusion in a poro-elastic half-space

L. MANTILONI(1)(2)

(1) *GFZ German Research Centre for Geosciences - Potsdam, Germany*
(2) *Department of Physics and Astronomy, Alma Mater Studiorum, University of Bologna Bologna, Italy*

received 31 January 2021

Summary. — Hydrothermal regions experience various phenomena, including ground deformation and, in the case of calderas, interaction between deep magmatic processes and shallow aquifers. The present work considers a source model consisting of a disk-shaped thermo-poro-elastic inclusion subject to a sudden change of temperature and pore pressure, embedded in a homogeneous poro-elastic half-space. We compare semi-analytical solutions for surface displacement with results from four other source models. The displacement components are similar to those of a spherical point-like source for a certain choice of geometric parameters, while they differ from the other models. On the basis of this comparison, we interpret the results of inversions on ground deformation data of the 1982–1984 unrest episode at Campi Flegrei caldera, Italy, where the thermo-poro-elastic source provides the best fit.

1. – Introduction

Hydrothermal regions, sometimes associated with calderas, host a variety of observable phenomena, such as ground deformation, hot springs and seismicity (see, *e.g.*, the Yellowstone caldera, USA [1]; the Rabaul caldera, Papua New Guinea [2]; the Hengill volcanic system, Iceland [3]). They are a manifestation of heat and mass transfer towards the Earth's surface, due to convection of water and other fluids within the crust, and are generally connected with hydrothermal processes [4, 5]. Such processes involve temperature and pore-pressure changes of fluids flowing through permeable rocks, but they can also arise from the inflation/deflation or internal differentiation of a magma chamber, or the emplacement of a new magmatic body [6, 7]. For example, [8] proposed a conceptual model for ground deformation episodes where a magma volume at shallow depth cools and crystalizes, releasing pressurized magmatic fluids into a shallow hydrothermal system. This leads first to surface uplift and then subsidence, as the flux of fluids decreases

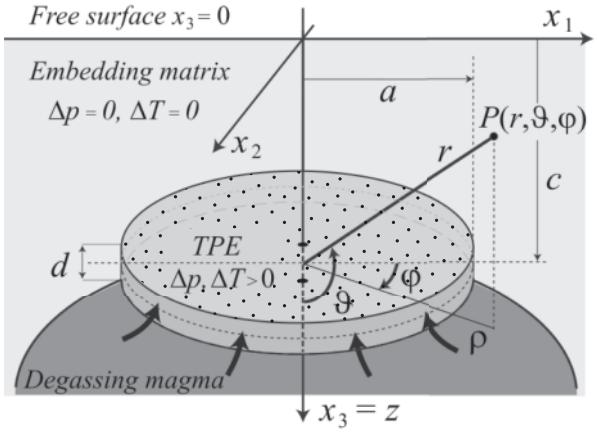

Fig. 1. – Scheme of the disk-shaped thermo-poro-elastic inclusion (dotted region), with radius a and thickness d. It is located at depth c and embedded in a poro-elastic half-space (light grey region). The inclusion undergoes sudden changes in temperature ΔT and pore pressure Δp caused by degassing of an underlying magma body (darker region). The median plane of the disk is drawn with a dotted line. The origin of both the spherical (r, θ, φ) and cylindrical (ρ, φ, z) references frames is at $x_1 = 0, x_2 = 0, x_3 = c$. (Modified from [13]).

over time or the rock permeability rapidly increases when the fluid pressure, exceeding the local strength of the crust, causes failures in the elastic matrix of the porous medium. Nonetheless, the discrimination between magmatic and hydrothermal processes is generally not trivial. Therefore, advancements in the modelling of these phenomena are of the essence in the comprehension of volcanic hazard.

Traditional approaches to ground deformation modelling in volcanic areas focus on the surface effects of a deformation source in the crust, which is usually a pressurized cavity representing a magma chamber or a sill (*e.g.*, a spherical source [9], a penny-shaped crack [10] or a spheroid [11]), although rectangular dislocations are also considered (*e.g.*, [12]). The source is typically embedded in a homogeneous, elastic half-space, and poro-elastic effects (that is, the presence of fluids within the rocks) are often neglected.

A recent work [13] has explored the mechanical effects induced by temperature and pore-pressure changes within a disk-shaped, horizontal Thermo-Poro-Elastic inclusion (which is referred to as "TPE" in the following, in accordance with [13]), embedded in an isothermal, poro-elastic half-space in free drainage conditions (fig. 1). Reference [14] already considered a spherical, shell-shaped TPE inclusion surrounding a magma chamber, embedded in an unbounded medium and representing a region of permeable rock being affected by a sudden increase in temperature and pore pressure. This is also the interpretation of the TPE source proposed in [13] (fig. 1). The authors, however, consider a disk-shaped inclusion, which can better describe a horizontal permeable rock layer injected with hot and pressurized fluids. More importantly, the free surface boundary condition is included: this is fundamental if we want to compare model predictions with measured surface displacement during an episode of unrest in a volcanic region.

In the following we summarize the main results of [13], which was applied to interpret the displacement field observed during the 1982–1984 unrest episode at Campi Flegrei caldera in southern Italy. By comparing forward models of displacement from the TPE semi-analytical solution with other four analytical solutions for magma-filled sources of deformation, we discuss the better fit obtained using the TPE source model.

2. – Methods

The constitutive relations of a thermo-poro-elastic medium [15] undergoing changes of stress τ_{ij}, temperature ΔT and pore pressure Δp are

$$e_{ij} = \frac{1}{2\mu}\left(\tau_{ij} - \frac{\nu}{1+\nu}\tau_{kk}\delta_{ij}\right) + \frac{1}{3H}\Delta p\delta_{ij} + \frac{1}{3}\alpha\Delta T\delta_{ij}, \tag{1a}$$

$$\tau_{ij} = 2\mu e_{ij} + \lambda e_{kk}\delta_{ij} - K\left(\frac{1}{H}\Delta p\delta_{ij} + \alpha\Delta T\delta_{ij}\right), \tag{1b}$$

where H is the Biot's constant, α the coefficient of thermal expansion, μ the rigidity, ν the drained isothermal Poisson's ratio and $K = 2\mu(1+\nu)/3(1-2\nu) = \lambda + \frac{2}{3}\mu$ the drained isothermal bulk modulus of the poroelastic medium. Following eq. (1a), the stress-free strain e^*_{ij} that the inclusion would sustain if the hosting medium was absent is given by:

$$e^*_{ij} = e_0\delta_{ij}, \quad \text{where} \;\; e_0 = \frac{1}{3H}\Delta p + \frac{1}{3}\alpha\Delta T. \tag{2}$$

As shown by [13], the displacement field in a point $\mathbf{x}$ can be obtained as

$$u_i(\mathbf{x}) = 3Ke_0 \int_{V_S} \frac{\partial G_{ik}}{\partial x'_k}(\mathbf{x}, \mathbf{x}')\mathrm{d}v(\mathbf{x}'), \tag{3}$$

where V_S is the volume of the TPE and G_{ik} is the elastic Green's tensor for a half-space with drained, isothermal elastic parameters [16].

On the other hand, the associated stress field τ_{ij} is provided by eq. (1b) and is defined separately within the inclusion, where $\tau_{ij} = \tau^{in}_{ij}$, and outside it, where $\Delta p = 0$, $\Delta T = 0$ and $\tau_{ij} = \tau^{out}_{ij}$, so that

$$\tau^{in}_{ij} = \lambda e_{kk}\delta_{ij} + 2\mu e_{ij} - 3Ke_0\delta_{ij}, \quad \tau^{out}_{ij} = \lambda e_{kk}\delta_{ij} + 2\mu e_{ij}, \tag{4}$$

with $e_{ij} = \frac{1}{2}\left(\frac{\partial u_i}{\partial x_j} + \frac{\partial u_j}{\partial x_i}\right)$. Since $G_{ik}(\mathbf{x}, \mathbf{x}')$ is singular within the inclusion, when $\mathbf{x} \to \mathbf{x}'$, we must take particular care when computing u_i, e_{ij} and τ_{ij} there.

The Cartesian components of the displacement field u_i are retrieved by first evaluating the sum of Green's tensor partial derivatives in eq. (3):

(5)

$$u_1 = 3KCe_0 \int_{-a}^{a} \mathrm{d}x'_1 \int_{-f(x'_1)}^{f(x'_1)} \mathrm{d}x'_2 \int_{c-\frac{d}{2}}^{c+\frac{d}{2}} \mathrm{d}x'_3 \; (x_1 - x'_1)\left\{\frac{1}{R_1^3} + \frac{(3-4\nu)}{R_2^3} - \frac{6x_3(x_3+x'_3)}{R_2^5}\right\},$$

$$u_2 = 3KCe_0 \int_{-a}^{a} \mathrm{d}x'_1 \int_{-f(x'_1)}^{f(x'_1)} \mathrm{d}x'_2 \int_{c-\frac{d}{2}}^{c+\frac{d}{2}} \mathrm{d}x'_3 \; (x_2 - x'_2)\left\{\frac{1}{R_1^3} + \frac{(3-4\nu)}{R_2^3} - \frac{6x_3(x_3+x'_3)}{R_2^5}\right\},$$

$$u_3 = 3KCe_0 \int_{-a}^{a} \mathrm{d}x'_1 \int_{-f(x'_1)}^{f(x'_1)} \mathrm{d}x'_2 \int_{c-\frac{d}{2}}^{c+\frac{d}{2}} \mathrm{d}x'_3 \left\{\frac{(x_3 - x'_3)}{R_1^3} - \frac{(3-4\nu)(x_3+x'_3)}{R_2^3} - \frac{6x_3(x_3+x'_3)^2}{R_2^5} + \frac{2x_3}{R_2^3}\right\},$$

where

$$R_1 = \sqrt{(x_1 - x_1')^2 + (x_2 - x_2')^2 + (x_3 - x_3')^2}, \tag{6}$$
$$R_2 = \sqrt{(x_1 - x_1')^2 + (x_2 - x_2')^2 + (x_3 + x_3')^2},$$
$$f(p) = \sqrt{a^2 - p^2}, \quad C = \frac{1 - 2\nu}{8\pi\mu(1-\nu)}$$

and the intervals of integration are the result of the geometry of the TPE (fig. 1). In the integrand functions in eq. (5) we can collect separately the terms depending on $\frac{1}{R_1^3}$, which diverge within the volume of the inclusion (V_s), and those depending on powers of $\frac{1}{R_2}$, which are bounded within V_s. For this reason, we refer to the terms depending on $\frac{1}{R_1^3}$ as *singular* terms (apex s), and to those depending on powers of $\frac{1}{R_2}$ as *non-singular* terms (apex ns).

The displacement field $\mathbf{u}$ is thus found by summing up two contributions:

$$\mathbf{u} = \mathbf{u}^s + \mathbf{u}^{ns}. \tag{7}$$

The singular contribution $\mathbf{u}^s$ can be interpreted as the gradient of a scalar potential Φ [13]:

$$\mathbf{u}^s = -\frac{e_1}{4\pi}\nabla\Phi, \quad \text{with} \quad \Phi(\mathbf{x}) = \int\limits_{V_S} \frac{1}{R_1}\mathrm{d}v(\mathbf{x}'), \quad \mathbf{e_1} = \mathbf{e_0}\frac{\mathbf{1}+\nu}{\mathbf{1}-\nu}. \tag{8}$$

The original volume integral in eq. (5) can be computed by expanding the potential Φ in Legendre polynomials [13], provided that the thickness d of the cylinder is much smaller than its radius a ($d/a \ll 1$).

It is possible to prove that the integrals of the *non-singular* terms in eq. (5) cannot be expressed as components of the gradient of a scalar potential as well, since the displacement field u^c as reported in eq. (5) is not irrotational (*e.g.*, [17]). Then, in [13] the non-singular components of displacement are obtained by performing analytical integrations and simplifying them into single integrals over one coordinate $\mathrm{d}x_i'$, which are computed numerically, yielding the *non-singular* contribution $\mathbf{u}^{ns}$ to $\mathbf{u}$.

The strain tensor $e_{ij} = e_{ij}^s + e_{ij}^{ns}$ can be also separated into a singular part, e_{ij}^s, and a non-singular one, e_{ij}^{ns}, related to derivatives of $\mathbf{u}^s$ and $\mathbf{u}^{ns}$, respectively. The singular components e_{ij}^s can be obtained analytically from spatial derivatives of the scalar potential Φ [13], while the non-singular ones are retrieved by analytical spatial derivatives of u^{ns} and semi-analytical computation of the corresponding integrals. The stress tensor τ_{ij} can then be retrieved both outside and within the TPE inclusion as in [13]. In eq. (5) it is worth noticing that displacement, strain and stress induced by a TPE source scale with the intensity e_0 of the isotropic stress-free strain, which in turn depends on the temperature and pore pressure change occurred within the inclusion due to the injection of magmatic fluids.

3. – The application to the 1982–1984 Campi Flegrei unrest

The caldera of Campi Flegrei (fig. 2(a)) is located west of the city of Naples, with an external diameter of about 14 km. The region has hosted volcanic activity since 47000 years ago [18], the last magmatic eruption (Monte Nuovo) dating back to 1538 AD [6], and has experienced several cycles of subsidence and uplift in historical times (*e.g.*, [6, 19]).

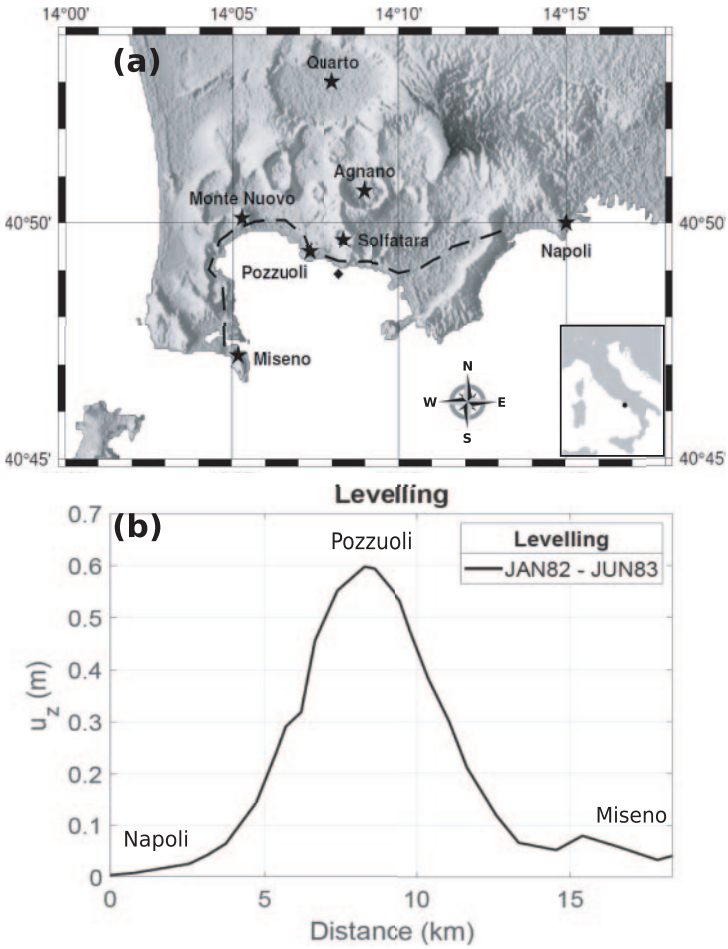

Fig. 2. – Map and deformation data of the studied area. (a) Map of the Campi Flegrei region. The black diamond represents the location of the centre of the deformation sources considered in the inversions. (b) Pattern of uplift measured between January 1982 and June 1983 on the baseline drawn in (a) as a dashed black line.

More recently, a major unrest episode in 1982–1984 marked the peak of a phase of uplift, after which a subsidence phase with much slower rates ensued. A new, ongoing trend of inflation started in 2005. Both these last phases have seen minor and rapidly recovered peaks of uplift over the long-term trend [20], and the shape of ground deformation (fig. 2(b)) has always remarkably maintained the same features of the 1982–1984 episode [21].

Different deformation sources have been applied to the 1982–1984 unrest over time: for instance, [22] envisaged a Mogi source at about 3 km depth beneath the centre of the caldera, while [23] and [24] considered pressurized penny-shaped horizontal cracks at a similar depth range. More recently, a mixed mode dislocation with both shear and tensile components was proposed by [25]. In most cases, these models advocated shallow (3–4 km deep) magmatic intrusions as the origin of both the 1982–1984 episode and the more recent ones [7, 26]. Purely magmatic models, however, cannot explain the long-

TABLE I. – *Results of the inversions and misfits for the models considered in* [13] *and the pCDM and Yang models considered here (in italics). In the case of Yang, "a" stands for the semi-major axis of the spheroid, while in the case of Mogi and TPE it stands for the radius of the respective sources. Parameters estimated by inversion of surface data are in bold. Both the TPE and the Yang spheroid have fixed aspect ratios $d/a = b/a = 0.3$, where "d" is the thickness of the TPE and "b" the semi-minor axis of the spheroid. For the pCDM, the parameter ΔV_r is the potency of the rectangular dislocations perpendicular to the horizontal axes, while ΔV_z is the potency of the one perpendicular to the vertical axis. The parameter $Q = \Delta P \cdot a^3(1-\nu)/\mu$ estimated for Mogi is the scaling factor for surface displacement. The value of ΔP for the Mogi model is retrieved from Q, while for the TPE Δp is retrieved from e_0, fixing $\Delta T = 100$ K. The misfit refers to the sum of the absolute difference between all the predicted and observed data.*

Model	c (km)	ΔV_r (m^3)	ΔV_z (m^3)	Q (m^3)	ΔP (MPa)	e_0	a (km)	Δp (MPa)	Total misfit (m)
TPE	**1.9**	–	–	–	–	$\mathbf{1.7{\cdot}10^{-3}}$	**1.9**	21	2.904
Mogi	**2.7**	–	–	$\mathbf{5.1 \cdot 10^6}$	64.1	–	–	–	3.868
Fialko	**2.9**	–	–	–	**3**	–	**2.5**	–	4.678
pCDM	**3.6**	$\mathbf{4.0{\cdot}10^6}$	$\mathbf{2.0{\cdot}10^7}$	–	–	–	–	–	4.722
Yang	**2.3**	–	–	–	–	–	**1.7**	**90**	7.649

lasting subsidence observed after the 1982–1984 peak [21], and both seismic tomography surveys [27] and deep drilling projects [28] found no evidence of shallow magma batches in the 3–4 km depth range [25].

Results of the inversion of geodetic data performed by [13] for the period June 1980 to June 1983 are reported in table I. For the TPE the aspect ratio in [13] was fixed to the value providing the minimum misfit ($d/a = 0.3$), as tests with different values found that smaller ratios require shallower and wider disks to reproduce the same data. In addition to the point-source approximation of a spherical pressurized source [9] and the penny-shaped crack [10] considered in the original work, here we perform a preliminary inversion with the point Compound Dislocation Model (pCDM) introduced by [12]: such model considers three mutually orthogonal rectangular dislocations that can reproduce deformation sources of any shape and orientation in space, and it can be useful in providing a first insight into the source geometry which is most likely for our case. The pCDM inversion retrieves the potencies ΔV_i of the three rectangular dislocations, which are the product of the area of the i-th dislocation and its opening (see [12]). We fixed the orientation of the dislocations and constrained the potencies of the two dislocations perpendicular to the horizontal axes so that they are equal ($\Delta V_1 = \Delta V_2 = \Delta V_r$; $\Delta V_3 = \Delta V_z$). This allows us to deal with an axisymmetric source in analogy with all the other models we consider, as well as with the same number of parameters of the TPE.

We also perform an inversion with a Yang source (*i.e.*, a vertically dipping prolate spheroid [11]) using a MatLab implementation of the "Libhalfspace" tool [29]. We chose to consider only three free parameters (namely, the semi-major axis, depth and overpressure of the spheroid) by fixing the ratio between the semi-minor (b) and semi-major (a) axes to the same value of the aspect ratio of the TPE (see also table I). In the following we refer to these models as Mogi, Fialko, pCDM and Yang, respectively, and the results of the new inversions are also reported in table I. We report here the expression for the components of displacement in cylindirical coordinates $(r; \phi; z)$ employed in [13] for the

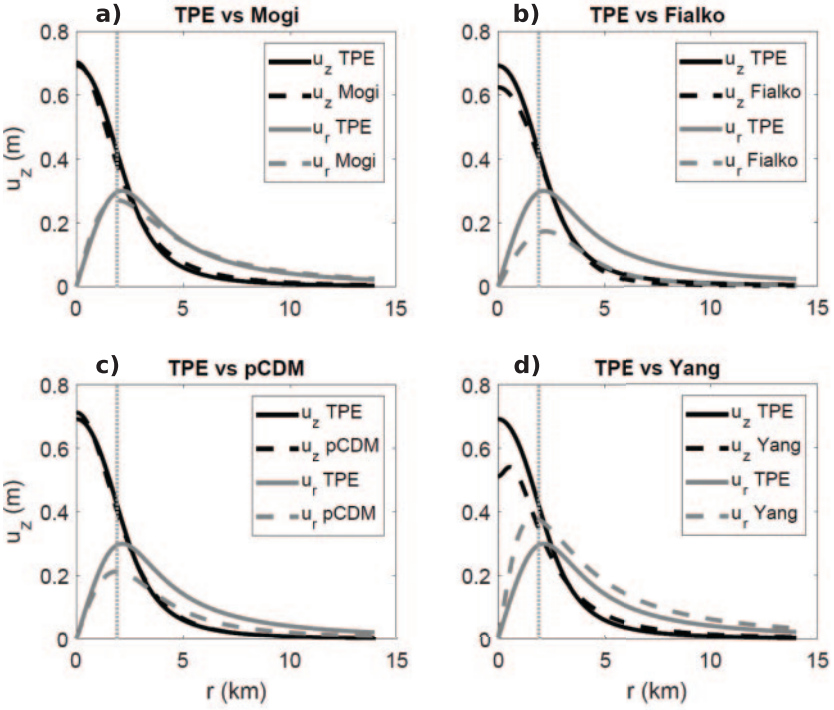

Fig. 3. – Comparison of vertical and radial components of surface displacement along a radial profile between the TPE and other four models applied to the 1982–1983 surface deformation data from Campi Flegrei (see fig. 2). The origin of the horizontal axes coincides with the source centre (black diamond in fig. 2), and the dotted vertical line marks the best-fit TPE radius. Best-fit values of the inverted parameters were employed for the different models (see table I).

Mogi model (see [9] and [30]):

$$u_r = \frac{\Delta P a^3}{4\mu}\left[\frac{r}{R_1^3} + f(r,z)\right], \tag{9a}$$

$$u_z = \frac{\Delta P a^3}{4\mu}\left[\frac{z-c}{R_1^3} + g(r,z)\right], \tag{9b}$$

with

$$f(r,z) = \left[\left(\frac{3K+7\mu}{3K+\mu}\right)\frac{r}{R_2^3} - \frac{6zr(z+c)}{R_2^5}\right], \tag{10a}$$

$$g(r,z) = \left[-\left(\frac{3K+7\mu}{3K+\mu}\right)\frac{z+c}{R_2^3} + \frac{2z}{R_2^3} - \frac{6z(z+c)^2}{R_2^5}\right], \tag{10b}$$

where ΔP is the overpressure of the Mogi source, a is the radius, c the depth of its centre and $R_1 = \sqrt{r^2+(z-c)^2}$, $R_2 = \sqrt{r^2+(z+c)^2}$ are the distances of the observation point from the source and the mirror source centres, respectively.

In order to understand the different ability of the models in reproducing data, we perform formal modelling of displacement at the Earth surface and compare (fig. 3) the horizontal and vertical components of the TPE to those of the other four models assuming the best-fit parameters reported in table I. Given the axial symmetry of the TPE with

respect to the vertical axis, the resulting displacement components for all the five models are referred to the cylindrical reference frame (r; ϕ; $z = x_3$) shown in fig. 1. Since the TPE results depend on poro-elastic parameters and pressure and temperature changes, it is important to recall how [13] fixed their values. The elastic parameters in isothermal and drained conditions of the poro-elastic matrix are set to $\lambda = 4$ GPa, $\mu = 6$ GPa ($\nu = 0.2$) as in [14]. The thermal expansion coefficient of the TPE is $\alpha = 3 \cdot 10^{-5}$ K^{-1}, while $H = 10$ GPa (see eq. (2)): both are characteristic of highly porous rocks [31], which constitute much of the upper stratigraphy of the Campi Flegrei caldera [8]. Finally, [13] considered typically $\Delta T = 100$ K within the TPE inclusion. A 100 K temperature jump is reasonable for the injection of overheated and overpressurized volatiles from a deep reservoir into a shallower system (fig. 1).

4. – Discussion and conclusions

We consider the disk-shaped TPE source embedded in a poro-elastic half-space which was proposed by [13] and compare the displacement it induces at the free surface to that of other four axisymmetric source models (pCDM, Mogi, Fialko and Yang), employing best-fit parameters (see table I) from inversions carried out in [13] and here on geodetic data from the 1982–1984 unrest episode at Campi Flegrei.

A first consideration involves the best-fit parameters retrieved for the pCDM model [12], that is, the potencies ΔV_r and ΔV_z. The latter is larger than the former by one order of magnitude. According to the definition of potency in [12] and bearing in mind that we assumed an axisymmetric source, the ratio $\frac{\Delta V_z}{\Delta V_r}$ is equal to the ratio between the semi-axis of the rectangular dislocation orthogonal to the $x_3 = z$ axis and the semi-axis of the one orthogonal to the x_1 (or equivalently, x_2) axis. This implies that the best-fit pCDM has a very flat geometry, comparable to that of a sill-like (Fialko) or disk-like (TPE) source, and, on the other hand, deems vertically elongated sources such as Yang unlikely to explain the observed surface deformation. This conclusion is corroborated by the value of the misfit for the Yang model in table I, and is compatible with the considerations of [32], who also applied a vertically dipping prolate spheroid to the same case study.

Results in table I show that the TPE provides the minimum misfit among the five models considered here and in [13]. An Akaike test (*e.g.*, [33]) shows that the increase in the number of parameters for the TPE with respect to Mogi, which yields the second lowest misfit, is justifed by the misfit improvement.

The displacement components evaluated for the TPE are in good agreement with those of Mogi (fig. 3(a)). Since Mogi-based models have already fit in good approximation the geodetic data at Campi Flegrei [26], the similarity between the Mogi and TPE results brings further evidence that the TPE cannot be ruled out in the interpretation of what caused the uplift.

The agreement is poorer in the case of Fialko (fig. 3(b)), especially for the horizontal component. Reference [13] discussed how, when employing best-fit values of parameters, the TPE reproduces well both horizontal and vertical data, while the Fialko model underestimates horizontal data (see [13], fig. 8). Even though our results do not involve comparison with the real data, the amplitude of the horizontal component of displacement predicted by the Fialko model is smaller than the one predicted by the TPE. It is worth mentioning that, according to [34], horizontal data have greater resolving power among different models. Moreover, since the decrease in amplitudes of displacement components away from the source centre is slower for the TPE than it is for Fialko, the TPE model may be better suited to describe situations with non-negligible horizontal de-

formation at considerable distances from the area of maximum uplift, without requiring a greater depth (table I).

There is good agreement also between the vertical displacement of the TPE and the pCDM, while the horizontal component for the pCDM follows a trend similar to the one of Fialko (fig. 3(c)). On the contrary, the comparison between TPE and Yang (fig. 3(d)) yields poor agreement for both components, especially close to the source centre.

Results of inversion in table I [13] show that in order to obtain 1/3 of the maximum observed surface uplift during the 1982–1984 unrest at Campi Flegrei, Mogi and Fialko sources require magma overpressures of $\Delta P = 64.1$ and 3 MPa, respectively, while the TPE disk requires a pore pressure change of $\Delta p = 21$ MPa, for a temperature change $\Delta T = 100$ K (for the same uplift, the requested Δp decreases with increasing ΔT, see eq. (2)). We also find that the overpressure required by the Yang source is $\Delta P = 90$ MPa. If we scale these pressure estimates by a factor of 3 to reproduce the maximum observed uplift in 1982–1984 (1.8 m) and compare them to lithostatic values at ≤ 3 km depth, we obtain unrealistically high magma overpressures for the Mogi and Yang sources ($\Delta P \approx 190$ and 270 MPa, respectively): such value for Mogi is compatible with previous estimates (*e.g.*, [22,30]). The same scaling also leads to unrealistically high pore-pressure changes Δp for the TPE, although it is to say that the maximum uplift scales also with the value of the thickness d, so that a larger aspect ratio $\frac{d}{a}$ could reproduce the maximum observed uplift with lower Δp. However, besides the hypothesis of small aspect ratios in the TPE model [13], results of the Yang model suggest that an aspect ratio larger than 1 is not in agreement with data. Fialko, instead, yields much lower overpressure estimation than all the other models ($\Delta P \approx 10$ MPa), as confirmed by previous works [24]. However, as also concluded in [13], the brittle rheology and temperatures met during deep drilling in nearby wells (400 °C at 3 km depth, *e.g.*, [28]) make the presence of a large magmatic reservoir at 2.9 km depth (table I) unlikely. On these grounds [13], excluded that the 1982–1984 uplift was due exclusively to the hydrothermal processes modeled by the TPE source, though it could be ascribed to the combined effects of such processes and the emplacement of magma at shallow depths [25]. Nonetheless, as concluded in [13], the TPE source could be suited for the modelling of recent, smaller uplift episodes ($\sim$ cm) at Campi Flegrei, most likely related to shallow hydrothermal processes [35].

Our model considers both poro-elastic and thermo-elastic effects. Temperature changes are more effective than pore-pressure changes in inducing strain due to the relative magnitudes of $\alpha\Delta T$ and $\Delta p/H$ in eq. (2). According to the TPE source scheme in fig. 1, [13] assumed the changes in Δp and ΔT to occur suddenly and uniformly over a specific volume (that is, the TPE inclusion) above the reservoir. Thus, the model neglects fluid migration and it is suited to estimate the contribution to ground deformation only during a given time interval.

Even though [13] and the present work have stressed the potential of the TPE to model hydrothermal processes, its solutions could be applied as well to mushy magmatic reservoirs dealing with injections of new magma, similar to what has been done in other works (*e.g.*, [36]).

It is to say that a remarkable difference bewteen the TPE and the other four models considered in [13] and here comes from the evaluation of the stress field, in that only the former envisages a non-vanishing shear stress component within the source itself. This promotes very different stress regimes at depth if compared to the other models, but is not evaluated here. A further limitation of the model presented by [13] arises from the hypothesis of a small aspect ratio, which limits the exploration of the internal region of the inclusion. Numerical modelling, however, as already tested in [13] and, recently,

in [37], can allow us to overcome the problem and enable the representation of TPE sources with arbitrary shapes. The same could be accomplished as well by considering multiple, closeby TPE disks with different size and values of e_0 (eq. (2)).

We conclude remarking that analytical models as those considered here are of critical importance in calibrating and assessing the validity of more complex numerical models. Their calculation speed also makes studying sensitivities, quantifying driving parameters and studying forecasts and their range of uncertainties much easier than with numerical models.

* * *

I wish to express my gratitude to an anonymous Reviewer, whose constructive remarks and suggestions have considerably improved the quality of the present work. I also wish to thank E. Rivalta, M. E. Belardinelli, M. Bonafede, M. Nikkhoo and M. Nespoli for some useful insights.

REFERENCES

[1] Tizzani P. *et al.*, *J. Geophys. Res. Solid Earth*, **120** (2015) 2627.
[2] Robertson R. M. and Kilburn C. R. J., *Earth Planet. Sci. Lett.*, **438** (2016) 86.
[3] Feigl K. L. *et al.*, *J. Geophys. Res. Solid Earth*, **105** (2000) 25655.
[4] Rinaldi A. P. *et al.*, *Phys. Earth Planet. Inter.*, **178** (2010) 155.
[5] Todesco M. A. *et al.*, *Geophys. Res. Lett.*, **41** (2014) 1471.
[6] Di Vito M. A. *et al.*, *Sci. Rep.*, **6** (2016) 32245.
[7] Macedonio G. *et al.*, *J. Geophys. Res. Solid Earth*, **119** (2014) 3986.
[8] Lima A. *et al.*, *Earth Sci. Rev.*, **97** (2009) 44.
[9] Mogi K., *Earthq. Res. Inst.*, **36** (1958) 99.
[10] Fialko Y. *et al.*, *J. Geophys. J. Int.*, **146** (2001) 181.
[11] Yang X.-M. *et al.*, *J. Geophys. Res. Solid Earth*, **93** (1988) 4249.
[12] Nikkhoo M. *et al.*, *Geophys. J. Int.*, **208** (2017) 877.
[13] Mantiloni L. *et al.*, *J. Volcanol. Geotherm. Res.*, **403** (2020) 107011.
[14] Belardinelli M. E. *et al.*, *Earth Planet. Sci. Lett.*, **525** (2019) 115765.
[15] McTigue D. F., *J. Geophys. Res. Solid Earth*, **91** (1986) 9533.
[16] Mindlin R. D., *Physics*, **7** (1936) 195.
[17] Jackson J. D., *Classical Electrodynamics* (Wiley) 1999.
[18] De Vivo B. (Editor) *Volcanism in the Campania Plain: Vesuvius, Campi Flegrei and Ignimbrites*, Vol. **9** (Elsevier Science) 2006.
[19] Di Vito M. A. *et al.*, *J. Volcanol. Geotherm. Res.*, **91** (1999) 221.
[20] Gaeta F. S. *et al.*, *J. Geophys. Res. Solid Earth*, **108** (2003) 2363.
[21] Troise C. *et al.*, *Earth Sci. Rev.*, **188** (2018) 108.
[22] Berrino G. *et al.*, *Bull. Volcanol.*, **47** (1984) 187.
[23] Battaglia M. *et al.*, *Geophys. Res. Lett.*, **33** (2006) L01307.
[24] Amoruso A. *et al.*, *Earth Planet. Sci. Lett.*, **272** (2008) 181.
[25] Trasatti E. *et al.*, *Earth Planet. Sci. Lett.*, **306** (2009) 175.
[26] Dvorak J. J. and Berrino G., *J. Geophys. Res. Solid Earth*, **96** (1991) 2309.
[27] Judenherc S. and Zollo A., *J. Geophys. Res. Solid Earth*, **109** (2004) B10312.
[28] Carlino S. *et al.*, *Renew. Sustain. Energy Rev.*, **16** (2012) 1004.
[29] Ferrari C. *et al.*, *Comput. Geosci.*, **96** (2016) 136.
[30] Bonafede M. and Ferrari C., *Tectonophysics*, **471** (2009) 4.
[31] Rice J. R. and Cleary M. P., *Rev. Geophys.*, **14** (1976) 227.
[32] Bianchi R. *et al.*, *J. Geophys. Res. Solid Earth*, **92** (1987) 14139.
[33] Hurvich C. M. and Tsai C.-L., *Biometrika*, **76** (1989) 297.
[34] Dieterich J. H. and Decker R. W., *J. Geophys. Res.*, **80** (1975) 4094.
[35] D'Auria L. *et al.*, *J. Geophys. Res. Solid Earth*, **116** (2011) B04313.
[36] Liao Y. *et al.*, *J. Geophys. Res. Solid Earth*, **123** (2018) 9376.
[37] Nespoli M. *et al.*, *J. Volcanol. Geotherm. Res.*, **415** (2021) 107269.